A COMBINED LAYOUT OPTIMIZATION WITH AN H-ADAPTIVE PROCEDURE APPLIED TO PLATE PROBLEMS

João. Carlos Arantes. Costa Jr.
Dep. Mechanical Eng., UFRN, CEP 59072-970, Natal, RN, Brasil
arantes@ufrnet.br

Marcelo Krajnc Alves
Dep. Mechanical Eng., UFSC, CEP 88040-970, Florianópolis, SC, Brasil
krajnc@emc.ufsc.br

Hilbeth Azikri Parente de Deus
Dep. Mechanical Eng., UFSC, CEP 88040-970, Florianópolis, SC, Brasil
azikri@emc.ufsc.br

Abstract. *The work proposes a new and competitive procedure for the determination of the optimum topology and shape of moderately thick plates. The basic idea concerning the proposed procedure is to combine, in an effective way, a composite material approach to topology optimization with a suitable h-adaptive mesh refinement scheme. This allows the simultaneous determination of the optimal topology and shape of plate structures. The optimization problem consists in the minimization of the compliance of the structure, subjected to volume, side and slope constraints. The Mindlin-Reissner plate theory is used with a locking-free element, based on the Discrete Shear Gap (DSG) approach. The proposed procedure lead to: The improvement of the resolution of the material/void interface, generating a refined optimal shape, associated with the final optimal topology; The considerable reduction in the total number of design variables relative to the specified final resolution of the optimal topology, when compared with the classical usage of homogeneous pixel type of mesh generally employed; and The decrease of the solution error of the plate problem, with the proper refinement of the elements, whose average error is larger than a given percentage of the global average error.*

Keywords: Topology optimization, Shape optimization, Error estimator, Mesh refinement, H-adaptive.

1. Introduction

Different variations of the composite material approach have been proposed in order to solve minimum compliance problems, as seen in Bendsoe (1995), Sigmund and Petersson (1998) and Petersson and Sigmund (1998). Some of these works had focused their attention in the determination of the optimal topology or reinforcement of plate problems, as seen in Bendsoe and Díaz (1993), Díaz *et al.* (1995), among others. However, most of these works were unable to generate a well-defined topology and in general, they presented a poor definition of the shape associated with the optimal topology. As a result, some innovative strategies were proposed with the objective of deriving not only the optimal topology but also the associated optimal shape of the structure. One of these strategies, proposed by Bendsoe and Rodrigues (1991), is the sequential solution of a topology optimization followed by a shape optimization problem. A serious drawback to this approach is the difficulty to automatically identify the material/void interface, resulting from the topology optimization problem. This difficulty is due to the presence of regions with intermediate relative densities, which may lead to an ambiguous interpretation of the final optimum topology. Another strategy, employed by Schwarz *et al.* (2001) and Costa and Alves, (2003), is the combination of a topology optimization procedure with a mesh refinement scheme. This strategy formulates the problem as the solution of a sequence of topology optimization followed by a re-meshing procedure. In Schwarz *et al.* (2001), the re-meshing is performed once the material regions are determined and their contours are approximated by splines curves. Now, in the redefined material regions is generated a new finer mesh. Here, again, the difficulty to automatically identify the material/void interface impairs the applicability of the method.

In this work, the objective is to propose a new and competitive procedure, which is able to simultaneously determine both the optimal topology and shape of moderated thick plate structures. Here, a single field, $\rho(x)$, denoted as the relative density, also characterizes the microstructure, represented by the SIMP model Bendsoe and Sigmund (1999), Sigmund and Petersson (1998) and Petersson and Sigmund (1998), used in the composite material approach. Here, we consider the minimization of the compliance of moderated thick plate structures, subjected to a volume, side and slope constraints. The Galerkin finite element discretization employs a Tri3 element, Costa (2003), that interpolates both the displacement and the relative density fields. Thus, the nodal values of the relative density, defined at each node of the mesh, define the design variables of the optimization problem. A local slope constraint is imposed in order to avoid the checkerboard instability problem and to reduce of the initial mesh dependency of the optimal topology. In addition, we

consider the classical Mindlin-Reissner plate theory and use a locking-free element, based on the Discrete Shear Gap (DSG) approach, see Bletzinger *et al.* (2000).

Here, Ω is the body domain with boundary $\partial\Omega = \Gamma_{\mathbf{u}} \cup \Gamma_{\mathbf{t}}$, $\Gamma_{\mathbf{u}} \cap \Gamma_{\mathbf{t}} = \varnothing$, $\Gamma_{\mathbf{u}}$ and $\Gamma_{\mathbf{t}}$ represent respectively the part of the boundary with a prescribed displacement, i.e. $\boldsymbol{u} = \overline{\boldsymbol{u}}$, and the part of the boundary with a prescribed traction load, i.e. $\boldsymbol{\sigma n} = \overline{\boldsymbol{t}}$. Moreover, $\overline{\mathbf{b}}$ is the prescribed body force and define the sets of admissible variations and displacements to be given respectively by $H_{\mathrm{o}} = \left\{ v_i \in \left[H^1(\Omega) \right]^2 \;\middle|\; \boldsymbol{v} = 0 \text{ on } \Gamma_{\boldsymbol{u}} \right\}$ and $H = \left\{ H_{\mathrm{o}} + \overline{\mathbf{u}} \right\}$.

2. Formulation of the problem

- **Reissner-Mindlin plate theory:** Here, we assume the displacement field $\boldsymbol{u}(\boldsymbol{x})$, to be expressed as: $\boldsymbol{u}(\boldsymbol{x}) = u_x \boldsymbol{e}_x + u_y \boldsymbol{e}_y + u_z \boldsymbol{e}_z$ where $\boldsymbol{e}_x$, $\boldsymbol{e}_y$ and $\boldsymbol{e}_z$ are the Cartesian base vectors, with

$$\begin{aligned} u_x(x,y,z) &= u(x,y) + z\theta_x(x,y) \;; \\ u_y(x,y,z) &= v(x,y) + z\theta_y(x,y) \;; \\ u_z(x,y,z) &= w(x,y) \;. \end{aligned} \tag{1}$$

As a result, the components of the infinitesimal strain tensor become:

$$\begin{aligned} \varepsilon_{xx} = \frac{\partial u}{\partial x} + z\frac{\partial \theta_x}{\partial x} = e^{\mathrm{o}}_{xx} + z\chi_{xx} \quad , \quad \varepsilon_{yy} = \frac{\partial v}{\partial y} + z\frac{\partial \theta_y}{\partial y} = e^{\mathrm{o}}_{yy} + z\chi_{yy} \quad , \quad \varepsilon_{zz} = 0 \;, \\ 2\varepsilon_{xy} = \gamma_{xy} = \left(\frac{\partial u}{\partial y} + \frac{\partial v}{\partial x} \right) + z\left(\frac{\partial \theta_x}{\partial y} + \frac{\partial \theta_y}{\partial x} \right) = \gamma^{\mathrm{o}}_{xy} + z\chi_{xy} \quad , \\ \gamma_{xz} = \theta_x + \frac{\partial w}{\partial x} \quad \text{and} \quad \gamma_{yz} = \theta_y + \frac{\partial w}{\partial y} \;. \end{aligned} \tag{2}$$

- **Microstructure model:** We consider the modeling of the material properties, at points with an intermediate relative density, to be done by the SIMP model. In this model the effective Young's modulus $E(\rho)$, is defined as $E(\rho) = \rho^{\eta} E_{\mathrm{o}}$. Here, E_{o}, denotes the Young's modulus of the fully dense material and, η, the penalization parameter, with $\eta = 4$. The homogenized constitutive equation, for the Mindlin-Reissner model, is given as $\boldsymbol{\sigma} = \left[\boldsymbol{D}^H(\rho) \right] \boldsymbol{\varepsilon}$ where $\boldsymbol{\sigma}^T = \left\{ \sigma_{xx}, \sigma_{yy}, \sigma_{xy}, \sigma_{xz}, \sigma_{yz} \right\}$ and $\boldsymbol{\varepsilon}^T = \left\{ \varepsilon_{xx}, \varepsilon_{yy}, \gamma_{xy}, \gamma_{xz}, \gamma_{yz} \right\}$, with

$$\left[\boldsymbol{D}^H(\rho) \right] = \begin{bmatrix} \left[\boldsymbol{D}^H_{11}(\rho) \right] & [0] \\ [0] & \left[\boldsymbol{D}^H_{22}(\rho) \right] \end{bmatrix}, \tag{3}$$

$$\left[\boldsymbol{D}^H_{11}(\rho) \right] = \frac{E(\rho)}{\left(1 - \nu_{\mathrm{o}}^2\right)} \begin{bmatrix} 1 & \nu_{\mathrm{o}} \\ \nu_{\mathrm{o}} & 1 \end{bmatrix}, \text{ and } \left[\boldsymbol{D}^H_{22}(\rho) \right] = G(\rho) \begin{bmatrix} 1 & 0 & 0 \\ 0 & 1 & 0 \\ 0 & 0 & 1 \end{bmatrix}. \tag{4}$$

The effective shear modulus, denoted by $G(\rho)$, is defined as

$$G(\rho) = \frac{E(\rho)}{2\left(1 + \nu_{\mathrm{o}}\right)}, \tag{5}$$

where ν_{o} is the Poison's coefficient of the fully dense material.

- **Generalized constitutive equations:** At this point, by defining the following generalized loads

$$\boldsymbol{N}^T = \left\{N_{xx}, N_{yy}, N_{xy}\right\} = \int_{-h/2}^{h/2} \left\{\sigma_{xx}, \sigma_{yy}, \sigma_{xy}\right\} dz \ ,$$
$$\boldsymbol{M}^T = \left\{M_{xx}, M_{yy}, M_{xy}\right\} = \int_{-h/2}^{h/2} \left\{\sigma_{xx}, \sigma_{yy}, \sigma_{xy}\right\} z\, dz \ , \tag{6}$$
$$\text{and} \quad \boldsymbol{Q}^T = \left\{Q_{xz}, Q_{yz}\right\} = \int_{-h/2}^{h/2} \left\{\sigma_{xz}, \sigma_{yz}\right\} dz \ ,$$

we are able to derive the generalized homogenized constitutive equations, given as:

• **Generalized membrane loading:**

$$\boldsymbol{N} = \left[\boldsymbol{D}_m\right]\boldsymbol{e}_m^{\circ}, \text{ where } \left\{\boldsymbol{e}_m^{\circ}\right\}^T = \left\{e_{xx}^{\circ}, e_{yy}^{\circ}, \gamma_{xy}^{\circ}\right\} \text{ and } \left[\boldsymbol{D}_m\right] = \begin{bmatrix} \left[\boldsymbol{D}_m^{11}\right] & 0 \\ 0 & D_m^{22} \end{bmatrix}, \tag{7}$$

$$\text{with } \left[\boldsymbol{D}_m^{11}\right] = \frac{E(\rho)h}{\left(1-\nu_{\circ}^2\right)}\begin{bmatrix} 1 & \nu_{\circ} \\ \nu_{\circ} & 1 \end{bmatrix} \quad \text{and} \quad D_m^{22} = G(\rho)h \ .$$

• **Generalized bending loading:**

$$\boldsymbol{M} = \left[\boldsymbol{D}_b\right]\boldsymbol{\chi}, \text{ where } \left\{\boldsymbol{\chi}\right\}^T = \left\{\chi_{xx}, \chi_{yy}, \chi_{xy}\right\} \text{ and } \left[\boldsymbol{D}_b\right] = \begin{bmatrix} \left[\boldsymbol{D}_b^{11}\right] & 0 \\ 0 & D_b^{22} \end{bmatrix}, \tag{8}$$

$$\text{with } \left[\boldsymbol{D}_b^{11}\right] = \frac{E(\rho)h^3}{12\left(1-\nu_{\circ}^2\right)}\begin{bmatrix} 1 & \nu_{\circ} \\ \nu_{\circ} & 1 \end{bmatrix} \quad \text{and} \quad D_b^{22} = G(\rho)\frac{h^3}{12} \ .$$

• **Generalized shear loading:**

$$\boldsymbol{Q} = \left[\boldsymbol{D}_b\right]\boldsymbol{\gamma}_t, \text{ where } \left\{\boldsymbol{\gamma}_t\right\}^T = \left\{\gamma_{xz}, \gamma_{yz}\right\} \text{ and } \left[\boldsymbol{D}_b\right] = G(\rho)h\begin{bmatrix} 1 & 0 \\ 0 & 1 \end{bmatrix}. \tag{9}$$

Now, with the consideration of the classical Mindlin-Reissner hypothesis, may be expressed as:

$$a(\boldsymbol{u},\boldsymbol{v}) = l(\boldsymbol{v}), \ \forall \ \boldsymbol{v} \in H_{\circ} \tag{10}$$

$$a(\boldsymbol{u},\boldsymbol{v}) = \int_{\Lambda} \left\{\boldsymbol{N}\cdot\boldsymbol{e}_m^{\circ}(\boldsymbol{v}) + \boldsymbol{M}\cdot\boldsymbol{\chi}(\boldsymbol{v}) + k\boldsymbol{Q}\cdot\boldsymbol{\gamma}_t(\boldsymbol{v})\right\} d\Lambda \ , \tag{11}$$

and

$$l\left(\boldsymbol{v}^{\circ}, \hat{\boldsymbol{\theta}}\right) = \int_{\Lambda} h\bar{\boldsymbol{b}}\cdot\boldsymbol{v}^{\circ}\, d\Lambda + \int_{\Gamma_t} \left\{\bar{\boldsymbol{N}}\cdot\boldsymbol{v}^{\circ} + \bar{\boldsymbol{M}}\cdot\hat{\boldsymbol{\theta}}\right\} d\Gamma \ , \tag{12}$$

where $k = 5/6$, $\boldsymbol{v} = \boldsymbol{v}^{\circ} + z\hat{\boldsymbol{\theta}}$, $\left\{\boldsymbol{v}^{\circ}\right\}^T = \left\{\hat{u}, \hat{v}, \hat{w}\right\}$, $\left\{\hat{\boldsymbol{\theta}}\right\}^T = \left\{\hat{\theta}_y, \hat{\theta}_x, 0\right\}$ and $\left\{\bar{\boldsymbol{N}}, \bar{\boldsymbol{M}}\right\} = \int_{-h/2}^{h/2} \left\{1, z\right\}\left\{\bar{t}_x(x,y,z)\boldsymbol{e}_x + \bar{t}_y(x,y,z)\boldsymbol{e}_y\right\} dz$.

• **Optimization problem:** The topology optimization problem can be stated as: Determine the relative density $\rho(\mathbf{x}) \in W^{1,\infty}(\Omega)$ that solves

$$\min_{\rho} l\left(\boldsymbol{u}(\rho)\right) \tag{13}$$

subjected to:

• **A volume constraint:** Let Ω denote the body domain and α a prescribed volume fraction, $\alpha \in (0,1)$, Then

$$\int_{\Omega} \rho \, d\Omega = \alpha \Omega \, . \tag{14}$$

• **Side constraints:** The relative density, ρ, is constrained to the set $[\rho_{\inf}, 1]$, with $\rho_{\inf} = 0.001$, i.e. $\rho \in [\rho_{\inf}, 1]$

• **Stability constraints:** With the objective to circumvent the checkerboard instability and to reduce the initial mesh dependency of the final optimal topology, we enforced a local slope constraint condition, i.e.,

$$\left(\frac{\partial \rho}{\partial x}\right)^2 \leq {C_x}^2 \text{ and } \left(\frac{\partial \rho}{\partial y}\right)^2 \leq {C_y}^2 . \tag{15}$$

These bounds are imposed component wise enabling us to properly impose symmetry conditions.

3. Description of the combined method

• **General description:** Here, general description of the procedure that combines the topology optimization method with a suitable *h*-adaptive mesh refinement scheme is presented. The most relevant characteristics of this approach are:

a) The improvement of the resolution of the material/void interface, defining properly the optimal shape associated with the resulting optimal topology;
b) The reduction of the initial mesh dependency of the final optimal topology;
c) The considerable reduction in the total number of design variables relative to the specified final resolution of the optimal topology;
d) The decrease of the solution error of the plate problem.

In this work, the total number of *h*-refinement steps is set a priori and to be applied and solve, at each step, a topology optimisation problem. The proposed procedure may be described as follows:

1. Read the initial finite element data structure
2. Read the initial value of the design variables
3. For each *h*-refinement step, do:
   - 3.1. Solve the topology optimisation problem
   - 3.2. Apply the mesh refinement procedure
     - 3.2.1. Read the mesh data structures
     - 3.2.2. Refine the finite element mesh
       - 3.2.2.1. Identify the elements that should be refined
       - 3.2.2.2. Perform the refinement of these elements and introduce the transition elements necessary to maintain the mesh compatibility
       - 3.2.2.3. Apply a constrained Laplacian smoothing procedure in order to improve the mesh quality
     - 3.2.3. Optimise the element nodal incidence in agreement with the scheme of storage of the linear system solver of source code.
     - 3.2.4. Update the mesh and the data structure of the finite elements

• **Mesh Refinement Strategy:** The strategy consists basically in: the identification of the set of elements that must be refined; their refinement and the introduction of the transition elements, employed with the objective of maintaining the mesh compatibility. The set of elements to be refined is determined with the usage of a pointer vector: $Pref(i), i = 1, ..., n_e$. The default value is $Pref(i) = 0$, representing no refinement. In case $Pref(i) = 1$, we proceed the refinement of the i-th element. This procedure is described as follows:

a) Set $Pref(i) = 0, i = 1, ..., n_e$.
b) For each element, determine the relative density at the baricenter, i.e., $\rho_i^{bar}, i = 1, ..., n_e$. If $\rho_i^{bar} \geq 0.4$, we denote the element as a "material" element and set: $Pref(i) = 1$. Otherwise, we denote the element as a "non-material" element. Based on these definitions, we define the material/void interface as the one obtained as a union of the common edges of two elements, one been a material element and the other a non-material element. In this step, we also identify the "material" elements that will be refined.
c) Determine the global and the elements average errors denoted respectively by Θ_G and Θ_e, $e = 1, ..., n_e$. Now, for each element we verify if $\Theta_e > (1+\varphi)\Theta_G$, for some given $\varphi > 0$. If true, we set $Pref(e) = 1$, i.e., the *e-th* element will be refined.

d) Determine the quality measure *Q* of each element in the mesh, given by $Q = \dfrac{6A}{\sqrt{3}\,L_{\max}\,P}$,where *A* is the area of the triangle, *P* is the one half of the perimeter of the triangle, $L_{\max} = \max\left\{\overline{ab}, \overline{ac}, \overline{bc}\right\}$ is the length of the element's largest side. Thus, for each element we verify: if $Q(e) \le 0.55$ then we set: $Pref\left(e\right) = 1$.

e) Identify all the "non-material" elements that have a face common with the material/void interface and set their pointer reference $Pref\left(e\right) = 1$. Thus, all "non-material" elements having a "material" element neighbour are also refined.

f) Perform an additional smoothing refinement criterion. Here, for each element whose $Pref\left(e\right) = 0$ we identify their neighbours. If the element has two or more neighbours whose $Pref\left(\circ\right) = 1$, then refine the given element, i.e., set $Pref\left(e\right) = 1$. The objective here is to avoid having a given non-refined element having two or more neighbours to be refined. This may lead to the generation of sharp edges in the material contour or may generate internal void regions with a poor material contour definition. Thus, we refine these elements.

• **Conditional Laplacian smoothing procedure:** In order to improve the mesh, after the refinement step, we employ a constrained Laplacian smoothing. The Laplacian process is conditional since it is only be implemented if the mesh quality of the set of elements improves. The mesh quality of the set of elements is defined as the quality of the worst element in the set; as seen in Costa and Alves (2003) and Costa (2003).

• **Error Estimator criteria:** Here, we make use of an error estimator based on a gradient recovery technique by means the energy norm. Let $\boldsymbol{\rho}$ be a realizable nodal relative density of the problem. The local displacement error is defined as: $\boldsymbol{e}(\boldsymbol{\rho}) = \boldsymbol{u}(\boldsymbol{\rho}) - \boldsymbol{u}^h(\boldsymbol{\rho})$ where $\boldsymbol{u}(\boldsymbol{\rho})$ and $\boldsymbol{u}^h(\boldsymbol{\rho})$ are the exact and approximate solution respectively. The energy norm is given by:

$$\left\|e(\boldsymbol{\rho})\right\|_{\mathrm{E}}^2 = \int_{\Omega} \boldsymbol{D}^H(\boldsymbol{\rho})\boldsymbol{\varepsilon}\left(\boldsymbol{e}(\boldsymbol{\rho})\right)\cdot\boldsymbol{\varepsilon}\left(\boldsymbol{e}(\boldsymbol{\rho})\right)d\Omega\,. \tag{16}$$

The local stress error may be expressed in terms of the local displacement error as:

$$\boldsymbol{e}_{\sigma}(\boldsymbol{\rho}) = \boldsymbol{\sigma}(\boldsymbol{\rho}) - \boldsymbol{\sigma}_h(\boldsymbol{\rho}) = \boldsymbol{D}^H(\boldsymbol{\rho})\boldsymbol{\varepsilon}\left(\boldsymbol{u}(\boldsymbol{\rho}) - \boldsymbol{u}_h(\boldsymbol{\rho})\right) = \boldsymbol{D}^H(\boldsymbol{\rho})\boldsymbol{\varepsilon}\left(\boldsymbol{e}(\boldsymbol{\rho})\right). \tag{17}$$

Therefore, we can rewrite the energy norm as:

$$\left\|\boldsymbol{e}(\boldsymbol{\rho})\right\|_{\mathrm{E}}^2 = \int_{\Omega}\left(\boldsymbol{\sigma}(\boldsymbol{\rho}) - \boldsymbol{\sigma}_h(\boldsymbol{\rho})\right)\cdot\left[\boldsymbol{D}^H(\boldsymbol{\rho})\right]^{-1}\left(\boldsymbol{\sigma}(\boldsymbol{\rho}) - \boldsymbol{\sigma}_h(\boldsymbol{\rho})\right)d\Omega\,. \tag{18}$$

Since the exact stress distribution is unknown, we approximate $\boldsymbol{\sigma}(\boldsymbol{\rho})$ by an improved solution $\boldsymbol{\sigma}^*(\boldsymbol{\rho})$, obtained by applying the projection technique, which is more, refined then $\boldsymbol{\sigma}_h(\boldsymbol{\rho})$. Thus, the error indicator is approximated as:

$$\left\|\boldsymbol{e}(\boldsymbol{\rho})\right\|_{\mathrm{E}}^2 = \int_{\Omega}\left(\boldsymbol{\sigma}^*(\boldsymbol{\rho}) - \boldsymbol{\sigma}_h(\boldsymbol{\rho})\right)\cdot\left[\boldsymbol{D}^H(\boldsymbol{\rho})\right]^{-1}\left(\boldsymbol{\sigma}^*(\boldsymbol{\rho}) - \boldsymbol{\sigma}_h(\boldsymbol{\rho})\right)d\Omega\,. \tag{19}$$

Now, once $\boldsymbol{\sigma}^*(\boldsymbol{\rho})$ is determined, we may compute the global average error Θ_G, as:

$$\Theta_G = \frac{1}{\Omega}\int_{\Omega}\left(\boldsymbol{\sigma}^*(\boldsymbol{\rho}) - \boldsymbol{\sigma}_h(\boldsymbol{\rho})\right)\cdot\left[\boldsymbol{D}^H(\boldsymbol{\rho})\right]^{-1}\left(\boldsymbol{\sigma}^*(\boldsymbol{\rho}) - \boldsymbol{\sigma}_h(\boldsymbol{\rho})\right)d\Omega \tag{20}$$

and the element average error, Θ_e, as

$$\Theta_e = \frac{1}{\Omega_e}\int_{\Omega_e}\left(\boldsymbol{\sigma}^*(\boldsymbol{\rho}) - \boldsymbol{\sigma}_h(\boldsymbol{\rho})\right)\cdot\left[\boldsymbol{D}^H(\boldsymbol{\rho})\right]^{-1}\left(\boldsymbol{\sigma}^*(\boldsymbol{\rho}) - \boldsymbol{\sigma}_h(\boldsymbol{\rho})\right)d\Omega_e\,. \tag{21}$$

4. Problem cases

Here, we present some problem cases with the objective of evaluating the performance of the proposed procedure. In order to show the evolution of the refinement strategy we illustrate some of the intermediate optimal topologies and their associated finite element meshes. For simplicity, we consider: The material Young Modulus $E_o = 215.0$ GPa and the Poisson's ratio $\nu_o = 0,3$. The thickness of the plate is $h = 0.01$ m.

• **Problem Case (1):** At this point, we consider the problem illustrated in Fig. 1, which consists of a plate clamped at all edges, submitted to a prescribed transversal load *P*=80.0kN on its centre and subjected to a prescribed volume fraction of $\alpha = 0.30$. Now, due to symmetry conditions, only one fourth of the domain was actually discretized.

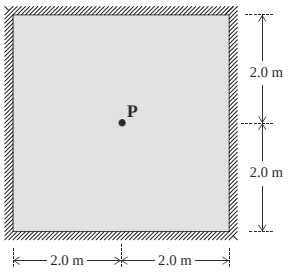

Figure 1. Plate clamped at all edges, submitted to a transversal load on its center.

The Fig. 2(a-f) show the sequence of meshes and associated optimum topologies resulting from problem case 1. The initial mesh, shown in Fig. 2(a), has 1410 elements and 756 nodes. The second mesh, shown in Fig. 2(b), has 3105 elements and 1635 nodes. The final mesh, shown in Fig. 2(c), has 9060 elements and 4665 nodes.

The Fig. 2(d-f) show the evolution of the partial optimal topologies showing the improvement of the definition of the associated optimal shapes. A similar topology, for this same class of problem, was obtained in Belblidia et al. (2001), employing their single layer model.

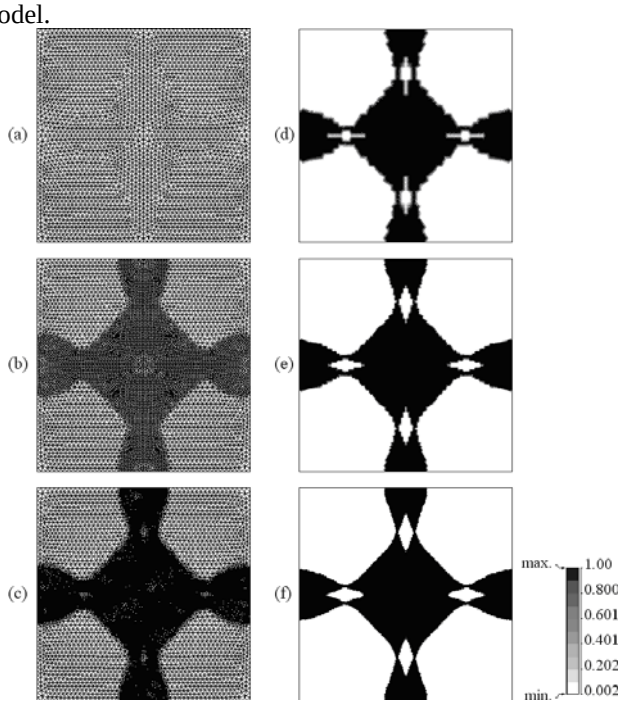

Figure 2. Sequence of optimal layouts – density level sets.

• **Problem Case (2):** consider the problem illustrated in Fig. 3, which consists of a plate, clamped on the left edge, submitted to a prescribed transversal load *P*=50.0kN on the middle of the right edge and subjected to a prescribed volume fraction of $\alpha = 0.30$. Now, due to symmetry conditions, only one-half of the domain was discretized.

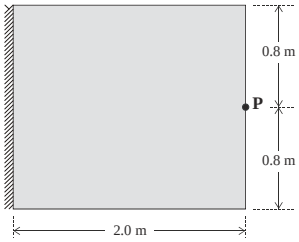

Figure 3. Plate clamped on the left edge, submitted to a transversal load on the middle of the right edge.

The Fig. 3(a-d) show the sequence of meshes resulting from the topology problem. The initial mesh, shown in Fig. 3(a), has 780 elements and 431 nodes. The second mesh, shown in Fig. 3(b), has 1862 elements and 991 nodes. The third mesh, shown in Fig. 3(c), has 5395 elements and 2784 nodes. The final mesh shown, in Fig. 3(d), has 17848 elements and 9054 nodes. Here, these numbers refer to the actual discretized mesh, corresponding to one-half of the domain. The Fig. 3(e-h) show the evolution of the partial optimal topologies. Again, a well-defined optimal shape is shown in Fig. 3(h).

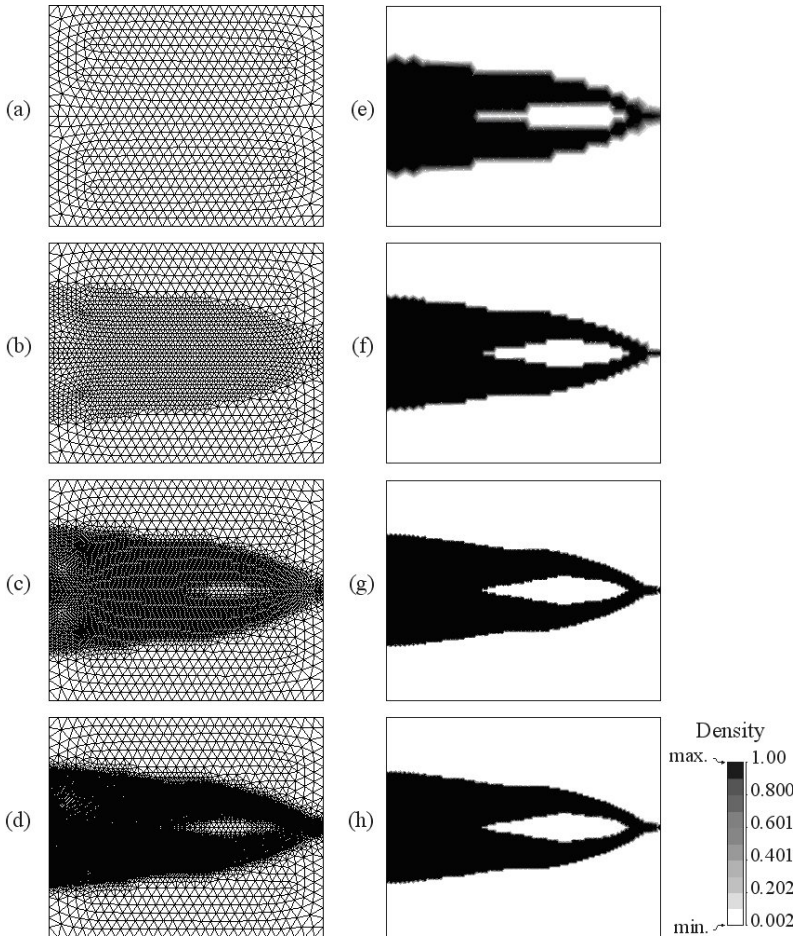

Figure 4. Sequence of optimal layouts.

5. Conclusions

The proposed algorithm has shown to be effective to obtain the optimum topology and shape of moderated thick plate structures. The imposition of a local slope constraint has shown to circumvent the checkerboard instability problem. The stability assured by the imposition of the slope constraint allowed us to employ a low order element, more specifically a Tri3 element, which together with the Discrete Shear Gap approach has reduced considerably the computational cost for solving large-scale plate problems. Furthermore, the usage of a suitable *h*-adaptive mesh refinement scheme has lead to:

- The improvement of the resolution of the material/void interface, generating a refined optimal shape, associated with the final optimal topology;
- The considerable reduction in the total number of design variables relative to the specified final resolution of the optimal topology, when compared with the classical usage of homogeneous pixel type of mesh generally employed;
- The decrease of the solution error of the plate problem, with the proper refinement of the elements, whose average error is larger than a given percentage of the global average error.

It is also important to notice that, in all problem cases, once the initial mesh has been defined, the resulting sequence of partial optimal topologies, obtained with the proposed *h*-adaptive mesh refinement procedure, has shown to convergence to a final optimal topology, with a well-defined optimal shape.

This new proposed procedure has lead to a very promising tool for the determination of the optimum topology and shape of plate compliance problems. The tool has shown to be very robust, computationally efficient, able to generate optimal topologies with undoubtedly optimal shapes and has shown no initial mesh dependency to the final optimal topology, which are the main requirements desired for commercial design tools.

6. Acknowledgements

The support of the CNPq – Conselho Nacional de Desenvolvimento Científico e Tecnológico – is gratefully acknowledged. Grant Numbers: 304020/2003-6.

The support of Prof. Krister Svanberg, from the Royal Institute of Technology, Stockholm, Sweden, that graciously provided the MMA solver.

7. References

Belblidia F, Lee JEB, Rechak S, Hinton E. Topology optimization of plate structures using a single or three-layered artificial material model. Advances in Engineering Software 2001; **32**: 159-168.

Belblidia F, Hinton E. Fully integrated design optimization of plate structures. Finite Element Analysis and Design 2002; **38**: 227-244.

Bletzinger KU, Bischoff M, Ramm E. A unified approach for shear-locking-free triangular and rectangular shell finite elements. Computers & Structures 2000; **75**: 321-334.

Bendsoe MP, Rodrigues HC. Integrated topology and boundary shape optimization of 2-D solids. Computer Methods in Applied Mechanics and Engineering 1991; **87**: 15-34.

Bendsoe MP, Díaz AR, Optimization of material properties for Mindlin plate design. Structural Optimization 1993; **6**: 268-270.

Bendsoe MP. Optimization of Structural Topology, Shape, and Material. Springer-Verlag: Berlin Heidelberg, 1995, 271p.

Bendsoe MP, Sigmund O. Material interpolation schemes in topology optimization. Archive of Applied Mechanics 1999; **69**: 635-654.

Costa Jr JCA, Alves MK. Layout optimization with *h*-adaptivity of structures. International Journal for Numerical Methods in Engineering 2003; **58**(1): 83-102.

Costa Jr JCA, Otimização topológica com Refinos H-adaptativos, PhD thesis, Universidade Federal de Santa Catarina, Florianópolis, Brazil, 2003.

Díaz AR, Lipton R, Soto CA. A new formulation of the problem of optimum reinforcement of Reissner-Mindlin plates. Computer Methods in Applied Mechanics and Engineering 1995; **123**: 121-139.

Petersson J, Sigmund O. Slope constrained topology optimization. International Journal for Numerical Methods in Engineering 1998; **41**: 1417-1434.

Schwarz S, Maute K, Ramm E. Topology and shape optimization for elastoplastic structural response, Computer Methods in Applied Mechanics and Engineering 2001; **190**: 2135-2155.

Sigmund O, Petersson J. Numerical instabilities in topology optimization: a survey on procedures dealing with checkerboards, mesh dependencies and local minima. Structural Optimization 1998; **16**: 68-75.

8. Responsibility notice

The authors are the only responsible for the printed material included in this paper.